Magnetic and magnetoelectric properties of self-assembled Fe2.5Mn0.504 nanocrystals

著者	Kohiki Shigemi, Okada Koichi, Mitome Masanori, Kohno Atsushi, Kinoshita Tomoki, Iyama Koichiro, Tsunawaki Fumiya, Deguchi Hiroyuki
journal or publication title	ACS Applied Materials & Interfaces
volume	3
number	9
page range	3589-3593
year	2011-08-26
URL	http://hdl.handle.net/10228/00006228

doi: info:doi/10.1021/am2008085

Magnetic and Magnetoelectric Properties of Self-assembled $Fe_{2.5}Mn_{0.5}O_4$ Nanocrystals

Shigemi Kohiki[†], Koichi Okada[†,‡], Masanori Mitome[§], Atsushi Kohno[#], Tomoki Kinoshita[†], Koichiro Iyama[†], Fumiya Tsunawaki[†], and Hiroyuki Deguchi[£]

[†]Department of Materials Science and [£]Department of Basic Science, Kyushu Institute of Technology, Kitakyushu 804-8550, Japan

[‡]Institute of Scientific and Industrial Research, Osaka University, Osaka 567-0047, Japan

[§]National Institute for Materials Science, Tsukuba 305-0044, Japan

[#]Faculty of Science, Fukuoka University, Fukuoka 814-0180, Japan

To whom correspondence should be addressed, kohiki@che.kyutech.ac.jp

ABSTRACT We report magnetoresistance of −40 %, corresponding to 80 % spin polarization, at magnetic field of 0.5 T and 200 K for oleic acid coated $Fe_{2.5}Mn_{0.5}O_4$ nanocrystals (FMO NCs) self-assembled on a SiO_2/Si substrate by drop casting fabrication. The FMO NCs exhibited spin glass

transition around 150 K and nonlinear current-voltage (*I-V*) characteristics. Fowler-Nordheim plot of the *I-V* characteristics indicated that electrons tunnel directly barriers between the FMO NCs. Transmission electron microscopy revealed that the FMO NCs are elongated hexagon in shape with size of ≈ 15 × 20 nm. The FMO NCs self-assembled in two-dimension hexagonal networks of collinear ferromagnetic moments. The [111] easy magnetization axis of each FMO NC was parallel to each other in the hexagonal arrays. Geometrically frustrated lattice of collinear ferromagnetic moments supports both a low and a high intergranular tunneling conductance for the self-assembled FMO NCs without and with magnetic fields, respectively.

KEYWORDS Low field magnetoresistance, Spin polarization, Magnetite-type $Fe_{2.5}Mn_{0.5}O_4$, Self-assembled nanocrystals, Oleic acid coating

INTRODUCTION

After findings of a large magnetoresistance (MR) for $LaMnO_3$ analogues [1,2], materials called half-metal including analogues of $LaMnO_3$ and Fe_3O_4 have been attracted great interest because of their possible 100 % spin polarized carriers promising for spintronics device applications. Half-metal oxides are conductor for one spin channel and insulator for the other spin channel. In the structure consisted of two ferromagnetic metal electrodes sandwiching a thin insulating barrier, the tunneling magnetoresistance (TMR) ratio is defined as TMR = $(R_{AP}-R_P)/R_P$, where R_{AP} and R_P are the resistances of the junction in the antiparallel and parallel configurations, respectively. A large TMR ratio of 1850 % was reported for $(La,Sr)MnO_3/SrTiO_3/(La,Sr)MnO_3$ junctions at 4.2 K, however the TMR ratio declined rapidly with rising temperature [3]. $(La,Sr)MnO_3$ is a half-metal with rather high Curie temperature $T_c \approx$ 360 K, while half-metal material with $T_c \geq 500$ K is requested for spintronics devices workable above room temperature (RT). Thus half-metal Fe_3O_4 ($T_c \approx 840$ K) and its analogues are suitable for such applications.

In the multiple junctions systems consisted of conducting ferromagnet NCs weakly contacted electrically one another via thin insulating barriers, the MR ratio is defined as MR = $(R_H - R_0)/R_0$, where R_H and R_0 are the resistances in applied field $H \neq 0$ and $H = 0$, respectively. Furthermore the MR ratio is connected to the spin polarization P of the material by MR ≡ $P^2/(1+P^2)$ [4]. The MR ratio of 50 % corresponds to P of 100 %. Zeng et al. [5] reported MR ratio of −35 % in H = 3.5 T at 60 K for an assembly of Fe_3O_4 NCs with diameter $\phi \approx 6$ nm. They reported that the NCs are superparamagnet with the blocking temperature of 40 K. Kant et al. [6] reported MR ratios of −11.5 % and −5.8 % with H = 1 T at 100 K for assemblies of Fe_3O_4 NCs ($\phi \approx 7.6$ nm) coated by SiO_2 and ZnO with thickness of ≈ 2 nm, respectively. They also reported that the NCs coated by SiO_2 and ZnO are superparamagnet with the blocking temperature of 200 K. Wang et al. [7] reported MR ratio of −40.9 % in H = 14 T at 110 K for an assembly of polystyrene coated Fe_3O_4 NCs with ϕ = 10 ~ 30 nm. Superparamagnetic systems of Fe_3O_4 NCs with randomly oriented magnetic easy axes displayed rather low MR ratio than that expected from almost complete spin polarization of the material. Therefore, control of intergranular relationship among the NCs is important to examine MR ratio intrinsic for the material.

Conductance of the magnetic tunnel junctions depends on the relative orientation of the half-metal NCs' magnetization, therefore controlling of the NCs' arrangement into hexagonal symmetry in two- and three-dimensions is crucial to the MR ratio for the half-metal NC arrays. The common way to build ordered architectures at the nanometer scale is the spontaneous self-assembly phenomenon [8]. Self-assembled half-metal NC arrays are known to represent an idealized granular magnetic material, in that the NC size, spacing, and density can be controlled with high precision. When we deposit drops of a monodisperse NC dispersion liquid with controlled concentration and allow the liquid to dry slowly on a substrate, NCs order in two-dimension hexagonal networks as a result of competition between the NC diffusion speed in the colloidal solution and the solvent evaporation speed.

We intended to fabricate hexagonal arrangement of single domain $Fe_{2.5}Mn_{0.5}O_4$ (FMO) NCs by drop casting method. The material FMO, an analogue of Fe_3O_4, is known as high T_C ferromagnetic oxide with *n*-type carriers. The MR ratio defined as $(G_0 - G_B)/G_B$, where G_0 and G_B are differential

conductance ($G = dI/dV$) without and with a magnetic field, respectively, of 150 % at RT was reported for the 50 nm width nanoconstrained structure of FMO [9].

In the first step, we synthesized monodisperse oleic acid coated FMO NCs [10]. We added oleic acid as stabilizing agent into organic solvent to prevent aggregation during FMO NC formation. Oleic acid, $CH_3(CH_2)_7CH{=}CH(CH_2)_7COOH$, is an unsaturated carboxylic acid with a *cis*-double-bond kink in the middle of its C_{18} tale. The polar head group chemisorbs to the hydrophilic NCs' surface and steric repulsion of the long chain prevents the NCs from agglomerating [11]. Since the FMO NCs coated with oleic acid are hydrophobic, we can readily prepare colloidal suspensions in non-polar organic solvent useful for the drop casting fabrication, and more the hydrophobization by oleic acid is highly advantageous for preventing the surface oxidation occurring even at RT, which is known to diminish observed spin polarization for Fe_3O_4 [12]. In the second step, we deposited drops of the FMO NCs suspension in hexane on a substrate and dried slowly for self-assembling of the NCs in hexagonal arrangement. Transmission electron microscopy (TEM) revealed that the [111] easy magnetization axis of each NC in hexagonal arrays aligned almost parallel one another. Therefore, we succeeded to fabricate the hexagonal lattice of collinear ferromagnetic moments of the FMO NCs.

Geometrical frustration among the collinear ferromagnetic moments of the self-assembled FMO NCs resulted in both a high and a low tunneling conductance under finite and zero magnetic fields, respectively. The FMO NCs showed spin glass transition with the freezing temperature T_F of 150 K based on the intergranular relationship among the NCs. The intermediate frustration lowers more or less the MR of the NCs hexagonal arrays. The low magnetic field ($H = 0.5$ T) MR of −40 % was observed at 200 K for the FMO NCs, the value corresponds to 80 % spin polarization.

EXPERIMENT

Synthesis of FMO NCs and Fabrication of Ordered Arrays by Self-assembly. FMO NCs were synthesized by slightly modified method of Kim et al. [10] from $Fe(acac)_3$ and $Mn(acac)_3$ in a solution of dibenzylether mixed with oleic acid. At first $Fe(acac)_3$, $Mn(acac)_3$, dibenzylether, and oleic acid,

weighed with the molar ratio of 5 : 1 : 157 : 12, were mixed with vigorous stirring for an hour at RT, and then the mixture was kept at 300 ºC for half an hour. After cooling to RT, NCs were precipitated from the crude solution by adding a mixed solvent of toluene/hexane (1:1) followed by centrifugation. Precipitated NCs were washed with anhydrous chloroform. The NCs were dispersed in a weak alkaline (pH = 10.4) aqueous solution. After stirring for 10 minutes, oleic acid with the molar ratio of [Fe] : [$C_{18}H_{34}O_2$] = 1 : 42 was added to the solution with vigorous stirring. After stirring for 20 minutes, 1N-HCl aqueous solution was added for neutralization of the solution. After removal of transparent solution, precipitated NCs surface coated with oleic acid were dispersed in hexane.

The as-synthesized NCs were used without post-preparative size-selection for fabrication of self-assembled nanostructure by drop casting on a SiO_2/Si substrate. The colloidal suspensions in hexane was dropped on a Si wafer covered with ≈140 nm thick SiO_2 layer, and then dried at 300 ºC for half an hour at 100 Pa. Pt electrodes with thickness of a few 100 nm were sputter deposited on surface of the casted FMO NCs layer.

Structural, Magnetic and Electric Characterization. The size and shape of as-synthesized FMO NCs were examined by using a JEOL JEM-3100FEF TEM operated at the electron acceleration voltage of 300 kV, and the crystal structure of the NCs was confirmed by x-ray diffraction (XRD) using a Rigaku CN2013 diffractometer with Cu *K*α radiation. For the FMO NCs/SiO_2/Si sample, the size, shape and arrangement of the NCs were examined by TEM, and the crystal structure of the NCs was reconfirmed by XRD.

For magnetic and electric characterization, we used a Quantum Design superconducting quantum interference devise magnetometer PPMS-5S. Diamagnetism from a SiO_2 layer was not compensated in any magnetization measurements. For temperature dependence of *dc* magnetization (*M*-*T*) measurement, the sample was cooled from RT to 5 K without field, then H = 100 Oe was applied. Zero-field-cooled (ZFC) magnetization was recorded with rising temperature up to 300 K. After the ZFC measurement, the sample was cooled again to 5 K in the same field, and then field-cooled (FC) magnetization was recorded with rising temperature to 300 K. For electrical measurement, Pt electrodes were bonded by

gold wires to the PPMS-5S system. At 200 K, current-voltage (*I*-*V*) characteristic without field was first measured, and then H = 0.01, 0.1, 0.15, 0.3, and 0.5 T were applied parallel to the current flow at each *I*-*V* measurement.

RESULTS AND DISCUSSION

TEM and XRD. TEM revealed that as-synthesized FMO NCs are elongated hexagon in shape with size of ≈ 15 × 20 nm, and the [111] axis of each NC are parallel to one another in the FMO NCs/SiO_2/Si sample. As seen in a TEM image of Fig. 1(a), as-synthesized FMO NC is single crystal with a lattice spacing of 0.49 nm. Such a lattice spacing is characteristic for the Fe_3O_4 (111) planes (JCPDS 19-0629). Thus the NCs enclosed by (111) planes are octahedron [13]. As well known for self-assembly fabrication, the FMO NCs ordered in two-dimension hexagonal networks in the FMO NCs/SiO_2/Si sample. As depicted in Fig. 1(b), a cross-sectional TEM image revealed that the NCs aligned hexagonally, and direction of the [111] easy magnetization axis of each NC is parallel one another. The Fast Fourier Transform (FFT) pattern for all the area of Fig. 1(b) is shown in Fig. 1(c), and distinctive FFT spots can be simulated well for magnetite type crystal structure. Splitting seen for each FFT spot indicates that orientation distribution of the [111] axis amounted to approximately ten degrees. However, the NCs ordered rather regularly than randomly in the FMO NCs/SiO_2/Si sample because the FFT pattern lacks the Debye-Scherer ring. The FMO NCs aligned parallel to the <111> direction in the region of approximately several hundred nanometers. For hexagonally arranged single domain FMO NCs shown in Fig. 1(d), geometrical frustration of collinear ferromagnetic moments is expected to bring about spin glass transition and a low intergranular electrical conductance with $H = 0$. In $H \neq 0$, ferromagnetic moment of the NCs align more parallel one another, and then the intergranular electrical conductance increases with an increase of H. Therefore, we expect to observe both spin glass transition and a high MR ratio for the FMO NCs/SiO_2/Si sample.

Figure 2 compares XRD patterns of the as-synthesized FMO NCs and the FMO NCs/SiO_2/Si sample. The as-synthesized NCs exhibited diffraction peaks in the upper panel, only attributable to cubic Fe_3O_4

crystal lattice with space group of Fd−3m (JCPDS 19-0629 a = 0.8396 nm for cubic cell). The FMO NCs/SiO_2/Si sample showed diffraction peaks in the lower panel, due to cubic Fe_3O_4 crystal lattice mentioned above and that from a Si wafer beneath the SiO_2 layer. The crystallite size of the FMO NCs/SiO_2/Si sample, estimated from half-width of the (311) reflection peak by using Scherer's equation, amounted to ≈15 nm which agrees with the NC size by TEM shown in Fig. 1(a).

Magnetic and Magnetoelectric Properties. Self-assembly of the FMO NCs gave rise to two-dimension hexagonal ordering of collinear ferromagnetic moments, which is expected to bring about magnetic frustration resulting in a large MR based on intergranular relationship. As shown by the inset of Fig. 3, the FMO NCs/SiO_2/Si sample demonstrated ferromagnetic behavior at 300 K in field dependence of magnetization (*M-H*). Sigmoidal *M-H* curve almost saturated above $H \approx 0.25$ T. Present sample consisting of single domain FMO NCs is ferromagnetic with the values of saturated magnetization $M_s = 0.4\ \mu_B$/cation, remnant magnetization $M_r = 0.01\ \mu_B$/cation, and coercive field $H_c = 6$ Oe.

Figure 3 demonstrates bifurcation of FC and ZFC magnetizations below 250 K. FC magnetization remained at almost constant below 250 K, whereas ZFC one fell off gradually with lowering the temperature. Such cooling history dependence of magnetization supports the structure of agglomerated ferromagnetic NCs, and suggests spin glass or superparamagnetic behavior in frequency dependence of magnetization.

Figure 4(a) shows in-phase (χ') and out-of-phase (χ") components of temperature-dependent *ac* susceptibility of the ZFC sample measured from 5 to 300 K on warming. In the χ'-*T* curve magnetic anomalies appeared around 250 K as a double cusp and around 150 K as a broad shoulder. Rather narrow peak around 250 K and broad peak around 100 K corresponding to the χ' anomalies are seen in the χ"-*T* curve. Although the temperature and height of the narrow χ" peak around 250 K stayed at constant despite the change in *f* from 1 to 10 Hz, those of the broad χ" peak around 100 K obviously increased and decreased with the increase of *f*, respectively. Such changes in χ" around 100 K are indicative of slow relaxation processes in spin glass or superparamagnetic materials [14]. The value of

the relative variation of the peak temperature (T_F) per decade of f for the χ" peak, $(\Delta T_F/T_F)/\Delta(\log_{10} f) = 0.06$, places the sample in the range of canonical spin glasses [15].

Thermal energy assists the reversal of magnetic moment in a single domain particle over the anisotropy energy barrier E_a. E_a is given by KV, where K is the effective magnetic anisotropy constant and V is the particle volume. In estimation of V we used diameter of 20 nm for present FMO NC. The relaxation time τ (= $2\pi f$) exhibits an exponential dependence on temperature represented by a Néel-Arrhenius law. Thus one obtain the equation $1/T_F = (-k_B/E_a)\{\ln(2\pi f) + \ln(\tau_0)\}$, where k_B is the Boltzmann constant and τ_0 is the pre-exponential factor. Since an inverse of T_F linearly shifted with a logarithm of f, the values of $E_a = 5.4 \times 10^{-20}$ J and $K = 1.4 \times 10^4$ J/m^3 were obtained from the gradient, $\tau_0 = 5.5 \times 10^{-17}$ sec from the intercept of the straight line in a T^{-1} vs. ln$f$ plot. The τ_0 value is largely smaller than that typical for superparamagnet with the order of $10^{-9} \sim 10^{-11}$ sec [16], which indicates a finite interaction between the NCs in the sample. Since magnetic moments become progressively frozen with lowering temperature to T_F, the sample is in the intermediately frustrated magnetic state below 200 K and in the fully frustrated magnetic state below 100 K.

χ'- and χ"-T curves of the ZFC sample of oleic acid coated FMO NCs for the drop casting fabrication are shown in Fig. 4(b). Contrary to the χ' and χ" anomalies respectively around 150 K and 100 K for the FMO NCs/SiO_2/Si sample, oleic acid coated FMO NCs showed no anomalies due to magnetic frustration. The anomaly around 250 K observed commonly for both the FMO NCs/SiO_2/Si sample and oleic acid coated FMO NCs is based on freezing effect of oleic acid. The χ" anomaly around 30 K for oleic acid coated FMO NCs indicated $(\Delta T_F/T_F)/\Delta(\log_{10} f) = 0.14$, which places the sample in the range of superparamagnet [15]. Therefore, the FMO NCs/SiO_2/Si sample demonstrated the spin glass transition based on intergranular magnetic interaction.

As shown in the inset of Fig. 5, the FMO NCs/SiO_2/Si sample demonstrated nonlinear I-V characteristics at 300 K, which is typical for intergranular tunneling conductance mechanism [17]. Fowler-Nordheim plot shown in Fig. 5 revealed that electrons tunnel across the interface between two adjacent NCs. The barrier height Φ for electron tunneling of 0.47 eV was derived from the equation for

zero-bias limit, $\ln(I/V^2) \propto \ln(1/V) - [2s(2m_e)^{1/2}/\hbar]\Phi^{1/2}$, where s is the barrier thickness, and m_e is the electron effective mass [18].

The sample exhibited linear relationship for ln$G$ versus $T^{-1/2}$ above 200 K, as depicted by the straight line from liner fit in the upper panel of Fig. 6. The resistance below 200 K was rather high and stayed at almost constant. We have tested the $T^{-1/4}$ form expected for variable range hopping, however we found that ln$G$ could not be simulated well by such a law. Temperature dependent I-V measurements were performed below 300 K because the electrical conduction obeying the Pool-Frenkel mechanism is known to be highly temperature dependent [19]. The current ln$I$ stayed at constant notwithstanding changes in temperature 1/T, as shown by the lower panel of Fig. 6. Carrier transport in the sample is dominated by direct electron tunneling between the NCs.

Negative MR was observed for the sample. As shown by the inst of Fig. 7, G at 200 K became high and low in H = 0.5 T and 0 T, respectively. The MR ratio defined as $(G_0-G_H)/G_H$, where G_0 and G_H are differential conductance without and with H, respectively. The MR ratio at $H \leq 0.15$ T was rather small than that at $H \geq 0.3$ T, as shown in Fig. 7. The MR ratio at 200 K reached −40 % at H = 0.3 T, and stayed at almost constant up to H = 0.5 T. The MR saturated at $H \geq 0.3$ T, which is consistent to the saturation in the M-H curve above $H \approx 0.25$ T as shown in the inset of Fig. 3. The hexagonal arrangement of the FMO NCs involves antiparallel configuration of the ferromagnetic moments between adjoining NCs in the array. Consequently the electron tunneling probability remains at small in such a magnetically frustrated system. The tunneling conductance of electrons moving across insulating barrier is small for the sample in H = 0. Alternatively, applied H aligns the collinear ferromagnetic moments in the hexagonal lattice into parallel. Parallel configuration of the ferromagnetic moments between the NCs enhances the electron tunneling probability in the arrays, and results in enlarged electron tunneling conductance for the sample. Thus the magnetically frustrated sample leads to a large negative MR based on intergranular magnetic interaction.

From the MR $\equiv P^2/(1+P^2)$ equation connecting MR to P [4], the observed low-field (0.5 T) MR of −40 % at 200 K corresponds to 80 % spin polarization of the material. The MR of 50 % corresponds to

P of 100 %, which is possible for half-metal material at a low temperature. In Fig. 1(c), we see some fluctuation in preferred orientation of the [111] axis of each NC in hexagonal arrays, therefore spin-dependent conductance in H = 0 between adjacent FMO NCs still remains rather high due to imperfections in antiparallel configuration of ferromagnetic moments than that expected for perfect antiparallel configuration. Intermediate frustration of collinear ferromagnetic moments in the hexagonal lattice reduces the observed tunneling MR even if the FMO was half-metal material with P = 100 %.

CONCLUSIONS

Two-dimension hexagonal ordering of collinear ferromagnetic moments fabricated by self-assembly of the FMO NCs was used for exploring intrinsic P. The assembly provided nonlinear I-V characteristics typical for intergranular tunneling of electrons. The electrons tunnel across the insulating barrier of oleic acid that coated the surface of the NCs. Geometrically frustrated arrays of the NCs exhibited spin glass transition around 150 K due to intergranular magnetic interactions. TEM supported the hexagonal ordering of collinear ferromagnetic moment of the NCs. Due to spin dependent tunneling, magnetic frustration enlarged MR to −40 %. At 200 K, a large spin polarization (P = 80 %) was achieved even in the low field H = 0.5 T. FMO has the potential to play an important role in spintronic devices such a spin injector.

Acknowledgement. S. K thanks Professor M. Mito and Professor H. Tanaka for discussion, and Dr. H. Shimooka for support in this work.

FIG. 1 TEM image of an FMO NC coated with oleic acid (a). Dotted line surrounding the NC is a guide for eye. Cross-sectional TEM image of the FMO NCs/SiO_2/Si sample (b). FFT pattern (c) for all the area of the image (b). Indices of distinctive FFT spots with the incident beam direction along the [-2 1 1] axis are overlapped, and crystallographic orientation distribution (≈10°) is represented by crossed bars. Schematic representation of hexagonally ordered collinear ferromagnetic moments (d). The ferromagnetic moment of single domain FMO NCs align parallel to the <111> direction.

FIG. 2 XRD patterns of the as-synthesized FMO NCs (upper panel) and the FMO NCs/SiO_2/Si sample (lower panel).

FIG. 3 Field dependence at 300 K (the inset) and temperature dependence in H = 100 Oe of magnetization of the FMO NCs/SiO_2/Si sample.

FIG. 4 Temperature dependence of χ' and χ" for the FMO NCs/SiO_2/Si sample (a) and for oleic acid coated FMO NCs for the drop casting (b) in the *ac* field h = 3.8 Oe and at both the frequency f = 1 and 10 Hz.

FIG. 5 *I-V* characteristics measured at 300 K in H = 0 (the inset) and Fowler-Nordheim plot of the *I-V* curve.

FIG. 6 Temperature dependence of G at 0.4 V (upper panel) and ln$I$ versus 1/T plot (lower panel).

FIG. 7 G versus V plot in H = 0 and 0.5 T (the inset) and MR in H = 0.01, 0.1, 0.15, 0.3, and 0.5 T at 200 K.

REFERENCES AND NOTES

[1] Jin, S.: Tiefel, T. H.: McCormack, M.: Fastnacht, R. A.: Ramesh, R.: Chen, L. H. *Science* **1994**, 264, 413.

[2] Tokura, Y.: Urushibara, A.: Moritomo, Y.: Arima, T.: Asamitsu, A.: Kido, G.: Furukawa, N. *J. Phys. Soc. Jpn*. **1994**, 63, 3931.

[3] Bowen, M.: Bibes, M.: Barthélémy, A.: Contour, J. -P.: Anane, A.: Lemaître, Y.: Fert, A. *Appl. Phys. Lett*. **2003**, 82, 233.

[4] Inoue, J.: Maekawa, S. *Phys. Rev. B* **1996**, 53, R11927.

[5] Zeng, H.: Black, C. T.: Sandstrom, R. L.: Rice, P. M.: Murray, C. B.: Sun, S. *Phys. Rev. B* **2006**, 73, 020402(R).

[6] Kant, K. M.: Sethupathi, K.: Rao, M. S. R. *J. Appl. Phys*. **2008**, 103, 07F318.

[7] Wang, W.: Yu, M.: Batzill, M.: He, J.:Diebold, U.: Tang, J. *Phys. Rev. B* **2006**, 73, 134412.

[8] Prasad, B. L. V.: Sorensen, C. M.: Klabunde, K. J. *Chem. Soc. Rev*. **2008**, 37, 1871.

[9] Goto, K.: Kanki, T.: Kawai, T.: Tanaka, H.*Nano Lett*. **2010**, 10, 2772.

[10] Kim, D.: Lee, N.: Park, M.: Kim, B. H.: An, K.: Hyeon, T.*J. Am. Chem. Soc*. **2009**, 131, 454.

[11] Tadmor, R.: Rosensweig, R. E.: Frey, J.: Klein, J. *Langmuir* **2000**, 16, 9117.

[12] Rybchenko, S. I.: Fujishiro, Y.: Takagi, Y.: Awano, M.*Phys. Rev. B* **2005**, 72, 054424.

[13] Zhang, L.: Wu, J.: Liao, H.: Hou, Y.: Gao, S. *Chem. Commun.* **2009**, 4378.

[14] Doman, J. L.: Fiorani, D.: Trone, E. *Adv. Chem. Phys*. **1997**, 98, 283.

[15] Mydosh, J. A. *Spin Glasses: An Experimental Introduction* (Taylor & Frances, London, 1993).

[16] Goya, G. F.: Berquó, T. S.: Fonseca, F. C.: Morales, M. P. *J. Appl. Phys*. **2003**, 94, 3520.

[17] Simmons, J. G. *J. Appl. Phys*. **1963**, 34, 1793.

[18] Beebe, J. M.: Kim, B.: Gadzuk, J. W.: Frisbie, C. D.: Kushmerick, J. G. *Phys. Rev. Lett*. **2006**, 97, 026801.

[19] Sze, S. M. *Physics of Semiconductor Devices* (Wiley, New York, 1981).

TOC SYNOPSIS Schematic representation of self-assembled $Fe_{2.5}Mn_{0.5}O_4$ nanocrystals on a SiO_2/Si substrate. For Source and Drain electrodes in electric measurements, Pt was sputter-deposited on the surface. In electromagnetic measurement, the external field *H* was applied parallel to current between the S-D electrodes. Bright (left) and dark (right) field TEM images show arrays of the nanocrystals. The magnetoresistance approximately −40 % was achieved at 200 K even in a low applied magnetic field of 0.3 T.

FIG. 1 by S. K et al.

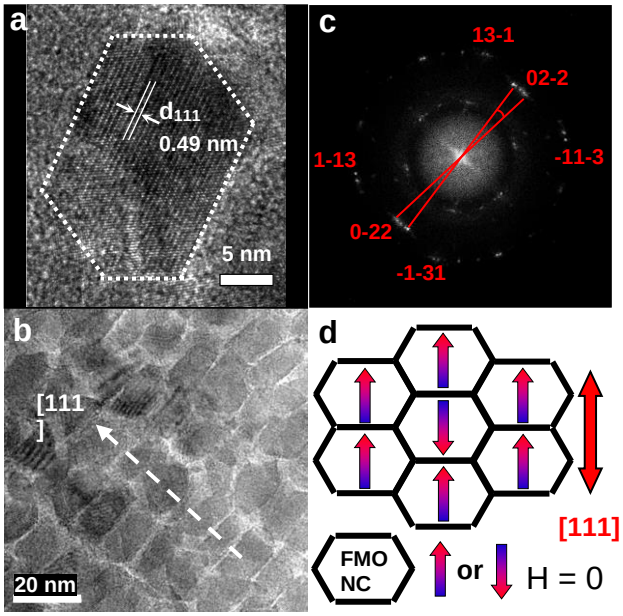

FIG. 2 by S. K et al.

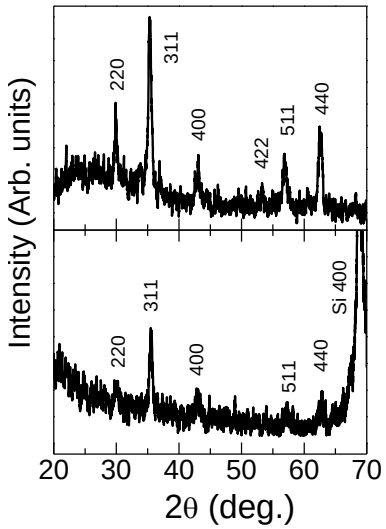

FIG. 3 by S. K et al.

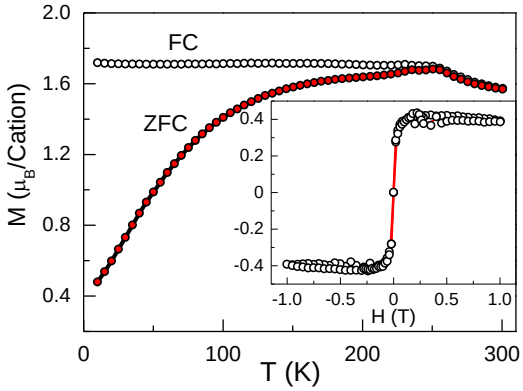

FIG. 4 by S. K et al.

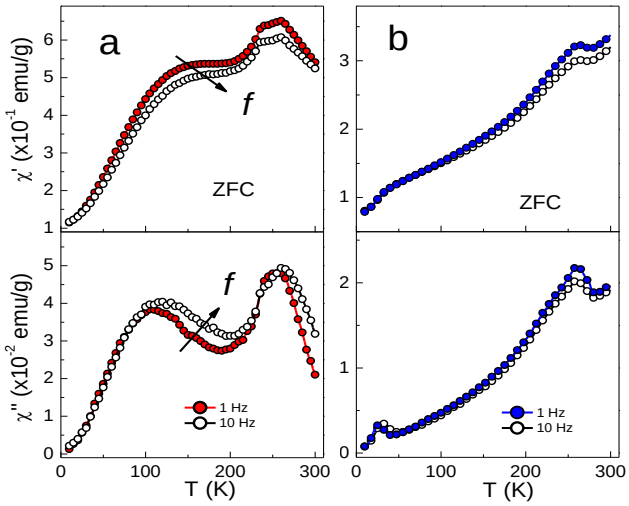

FIG. 5 by S. K et al.

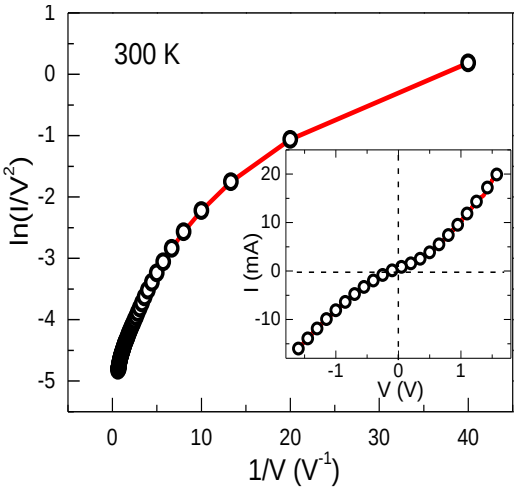

FIG. 6 by S. K et al.

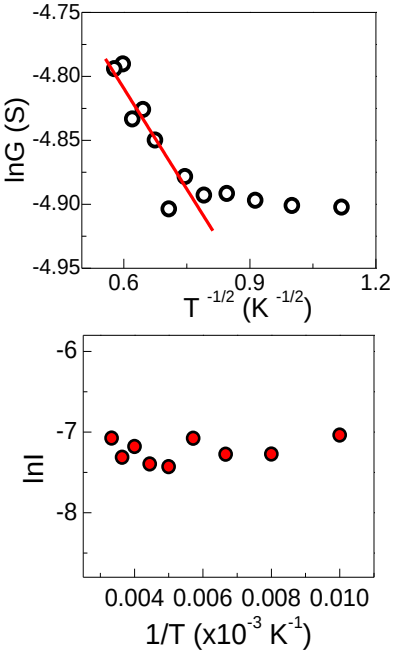

FIG. 7 by S. K et al.

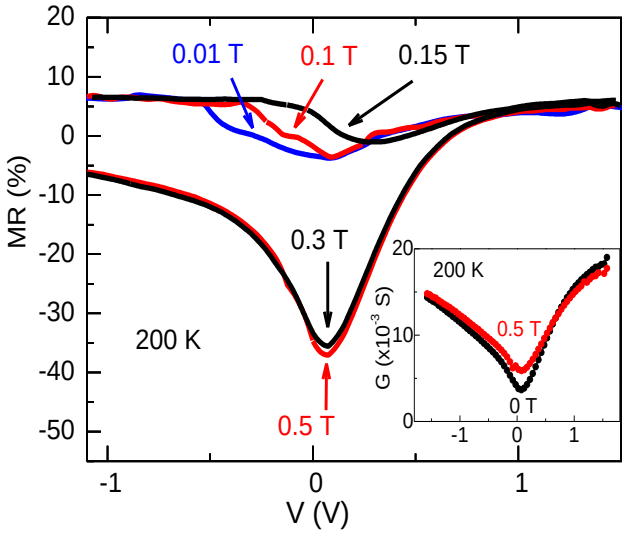

TOC

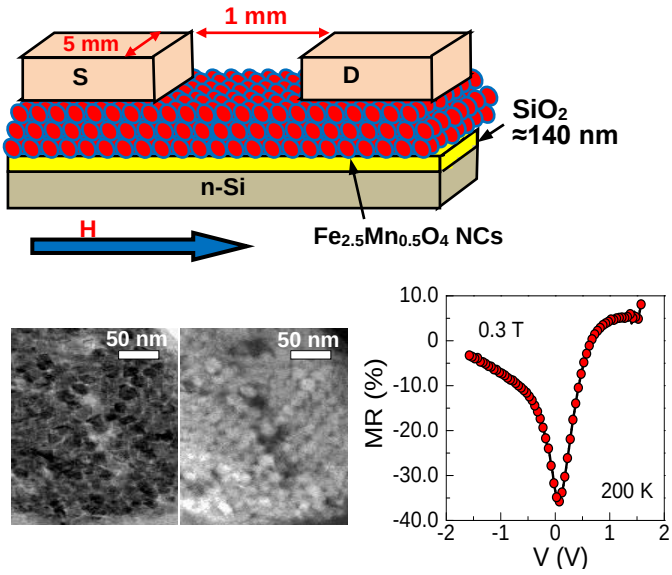
1 mm
5 mm
S
D
SiO2
≈140 nm
n-Si
H
Fe2.5Mn0.5O4 NCs
50 nm
50 nm
10.0
0
-10.0
-20.0
-30.0
-40.0
MR (%)
0.3 T
200 K
-2
-1
0
1
2
V (V)